Biocompatible, Biodegradable and Porous Liquid Crystal Elastomer Scaffolds for Spatial Cell Cultures[a]

Anshul Sharma,[†] Abdollah Neshat,[†] Cory J. Mahnen, Alek d. Nielsen, Jacob Snyder, Tory L. Stankovich, Benjamin G. Daum, Emily M. LaSpina, Gabrielle Beltrano, Yunxiang Gao, Shuo Li, Byung-Wook Park, Robert J. Clements, Ernest J. Freeman, Christopher Malcuit, Jennifer A. McDonough, LaShanda T. J. Korley, Torsten Hegmann, Elda Hegmann*

Here we report on the modular synthesis and characterization of biodegradable, controlled porous, liquid crystal elastomers (LCE) and their use as three-dimensional cell culture scaffolds. The elastomers were prepared by cross-linking of star block-co-polymers with pendant cholesterol units resulting in the formation of smectic-A LCEs as determined by polarized optical microscopy, DSC, and X-ray diffraction. Scanning electron microscopy revealed the porosity of the as-prepared biocompatible LCEs, making them suitable as 3D cell culture scaffolds. Biodegradability studies in physiological buffers at varying pH show that these scaffolds are intact for about 11 weeks after which degradation sets in at an exponential rate. Initial results from cell culture studies indicate that these smectic LCEs are compatible with growth, survival, and expansion of cultured neuroblastomas and myoblasts when grown on the LCEs for extended time periods (about a month). These preliminary cell studies focused on characterizing the elastomer-based scaffolds' biocompatibility and the successful 3D incorporation as well as growth of cells in 60 to 150-μm thick elastomer sheets.

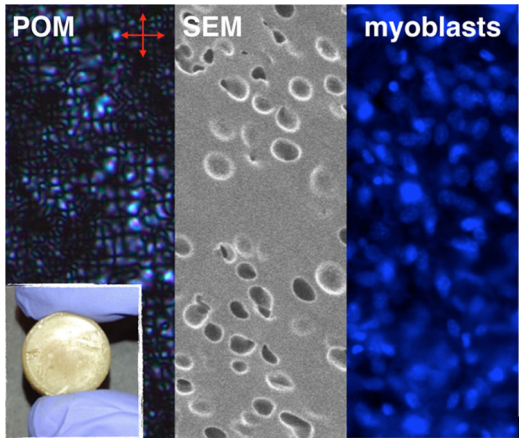

A. Sharma, Prof. T. Hegmann
Chemical Physics Interdisciplinary Program, Kent State University, Kent (OH) 44242, USA
A. Sharma, Dr. A. Neshat, Dr. Y. Gao, Prof. T. Hegmann, Prof. E. Hegmann
Liquid Crystal Institute, Kent State University, Kent (OH) 44242, USA
Fax: +330-672-2796; E-mail: ehegmann@kent.edu
C. J. Mahnen, A. D. Nielsen, J. Snyder, T. L. Stankovich, E. M. LaSpina, G. Beltrano, S. Li, Dr. B.-W. Park, Prof. R. J. Clements, Prof. E. J. Freeman, Prof. C. Malcuit, Prof. J. A. McDonough, Prof. E. Hegmann
Department of Biological Sciences, Kent State University, Kent (OH) 44242, USA
B. G. Daum, Prof. T. Hegmann, Prof. E. Hegmann
Department of Chemistry and Biochemistry, Kent State University, Kent (OH) 44242, USA
Prof. L. T. J. Korley
Macromolecular Science and Engineering Department, Case Western Reserve University, Cleveland (OH) 44106, USA
Prof. T. Hegmann
Department of Chemistry and Department of Pharmacology and Therapeutics, University of Manitoba, Winnipeg Manitoba R3T 2N2, Canada

[a]**Supporting Information** is available from the Wiley Online Library or from the author.
[†]These authors contributed equally to this work.

DOI: 10.1002/mabi.201400325

1. Introduction

Since the mid 1980's, the emerging field of tissue engineering using scaffolds has advanced considerably with significant efforts resulting in the development of implantable scaffolds consisting entirely of biomaterials. These scaffolds demonstrate promise for tissue engineering and are investigated as replacements for diseased or damaged tissues.[1] Typical cell culture models are hampered by their two-dimensional nature. Although cultured cells grown on a flat dish provide insights into cell processes, the relationships between spatially oriented cells are less obvious. Biomaterials and biocompatible synthetic polymeric scaffolds can be used to promote viability and differentiation of stem cells seeded inside, and both processes can be stimulated by the intrinsic properties of the scaffold and the incorporation of specific cues into the material.[2]

The combination of cells with polymeric scaffolds is a promising strategy for engineering tissues and cellular delivery.[3] Several types of scaffolds have been used in combination with cells for tissue engineering applications. Such scaffold materials can generally be classified as natural or synthetic and each have distinct advantages and drawbacks.[4] However, not many of these research strategies for creating new, more-adaptable scaffolds have yet demonstrated the use of biocompatible scaffolds that can, by choice, respond to a variety of external stimuli such as temperature, applied fields, surface alignment, or mechanic deformation (stress, strain) with a macroscopic ordering event (an increase in order). Such smart responsive scaffold would be able to report anisotropic growth of expanding cell lines back to the observer with an easily discernable optical response. Liquid crystalline materials would be an ideal platform for such cell scaffolds and fulfill most of these requirements listed above. However, biodegradable and biocompatible liquid crystal elastomers (LCEs) have not been reported thus far, but should in principle be easy to obtain if known biocompatible liquid crystal motifs are attached to a biocompatible and biodegradable elastomer backbone. LCEs have rather unique properties[5] and have been introduced as artificial muscles,[6] sensors,[7] and actuators[8] as well as used for tunable lasing[9] and light-driven motors.[10] The use as a porous scaffold for cell scaffolds would open up an entirely new area of application for LCEs, where the known properties of liquid crystals could be exploited to monitor cell attachment, proliferation, and even tissue regeneration.

To develop such new type of LCE-based scaffold for tissue engineering and biomedical applications, the scaffold must have well-defined porosity and surface properties that would provide support for cell adherence, growth, and transport of the nutrients and mass transport in and out of the scaffold pores under physiological conditions. Three types of mass transport have to be considered for 3D cell cultures: (a) oxygen mass transport (controlling metabolism rate), (b) mass transport of nutrients to cells, and (c) waste mass transport (eliminating toxins that, for example, raise pH to toxic levels, among others).[11] Not less important, elastomer porosity promotes 3D cell–elastomer interactions, space for extracellular matrix (ECM) formation and the possibility of linking molecular entities to allow binding of cell growth factors or other proteins to enhance cellular adhesion and ECM formation. Chemical and photo-initiated cross-linking of linear polymer precursors or multi-arm polyester precursors, also known as star shaped copolymers, have been used as methods for designing porous polymeric materials for biomedical applications. However, methods for the preparation of porous elastomers are rare. One example includes the incorporation of a leachable solid such as paraffin beads into a polymer and draining it after forming porous elastomer materials[12] or the use of a solvent vapor annealing method developed to prepare thin films of block copolymers with well-defined porosity.[13] Despite many advantages, these procedures have certain limitations. For example, photo-initiated cross-linking is limited to polyesters and it requires an extra step to attach an unsaturated moiety to polymers prior to cross-linking.[14] Another important factor in designing a biodegradable scaffold for tissue engineering applications is the degradation rate. Once *in vivo*, scaffolds should retain their structural integrity and biomechanical strength for a period of time enough for cell adherence, growth, and proliferation. The physical properties of elastomers can be tuned in a way to withstand mechanical tasks such as strain, stress, and impacts because they are soft, deformable,[15] and can be functionalized. They have also been found suitable as carriers for drug delivery applications. Biodegradable elastomers have mainly been made of two types; thermoplastics[16] and thermosets.[17,18] Thermoplastics are easily made; however, they degrade heterogeneously because of the presence of crystalline and amorphous regions within the material leading to a rapid loss of mechanical strength. While thermosets are not as easily prepared, they do offer more uniform biodegradation rates, better mechanical properties, and chemical resistance. Hence, thermoset elastomers based on three-arm star block co-polymers (SBCs)[19] using ring opening polymerization of the suitable monomers followed by liquid crystal functionalization and cross-linking to form a LCE were selected as the fundamental materials of choice for the preparation of the proposed cell matrices.

As a proof-of-concept, we here report the first synthesis, characterization and use of a biocompatible, biodegradable, and porous LCE by combining two lactone-based monomers and (D,L)-lactide into a cross-linkable star block copolymer (SBC). A modification of the method developed by Amsden et al.[13] was employed to allow for further modification of the SBC with halogen atom substitution at different

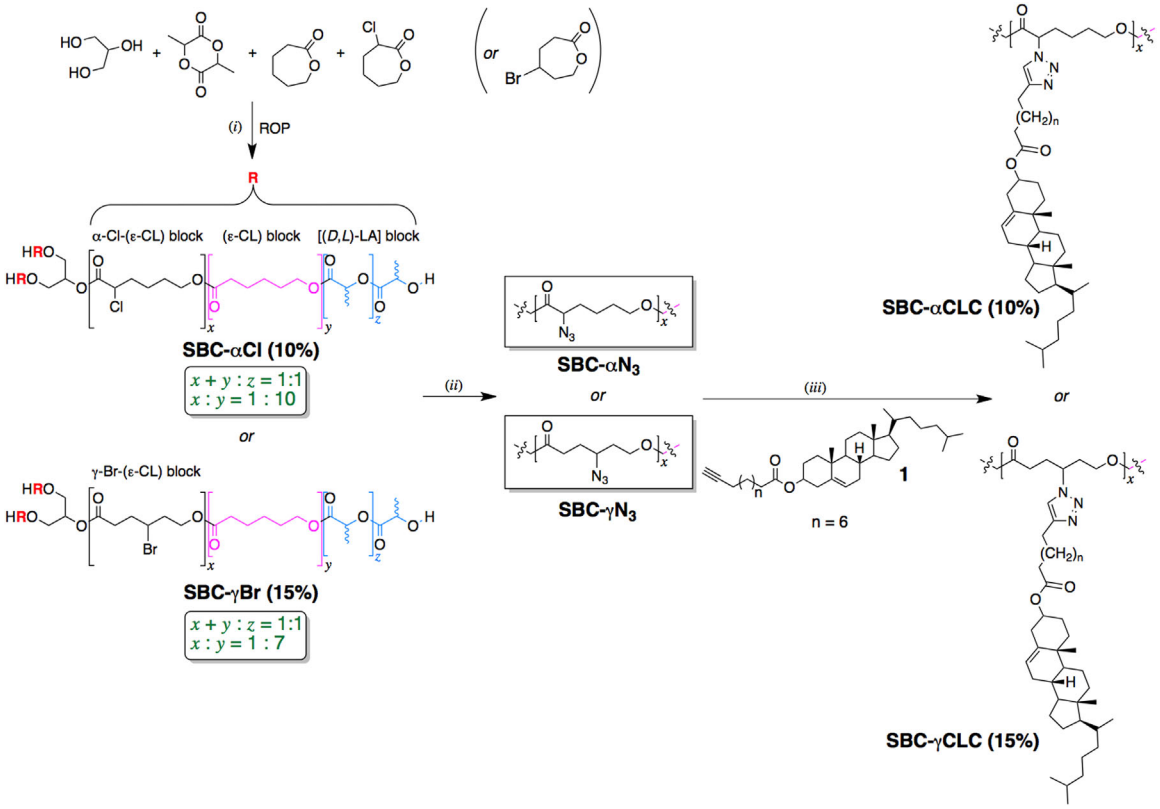

Scheme 1. Synthetic pathway to star block copolymers (SBCs) used for the preparation of SRS materials with biocompatible cholesterol liquid crystal pendants in the α position. Reactions and conditions: (*i*) $Sn(Oct)_2$, 140 °C (ROP: ring opening polymerization), (*ii*) NaN_3, DMF, and (*iii*) CuI, NEt_3, DMF.

positions of the block copolymers that would provide tunable flexibility of the liquid crystal pendant groups (α or γ to the carbonyl group). First, a three-arm star copolymer was synthesized by ring opening copolymerization of (D,L)-LA, ε-CL, and ε-CL with a halogen atom on either the α or γ carbon of the ε-CL monomer (Scheme 1). Displacement of the halogen atoms with azide groups generated block copolymers with straightforward access to liquid crystal functionalization (Scheme 1). The subsequent "click" reaction of cholesteryl 5-hexynoate **1** produces liquid crystal (LC) functionalized block copolymers. Cholesterol, was chosen as liquid crystal moiety because of its biocompatibility (cholesteryl benzoate isolated from carrots, for example, was among the first compounds to be found liquid crystalline), and because of its thermal stability needed during the cross linking for the subsequent preparation of LCEs at 140 °C for about 48 h. The morphology, thermal properties, and phase behavior of the final LCEs were first studied by scanning electron microscopy (SEM), polarized optical microscopy (POM), differential scanning calorimetry (DSC), thermogravimetric analysis (TGA), and small angle X-ray diffraction (SAXD). The mechanical properties were also assessed using tensile measurements, and the biodegradability tested in a buffer solution at different pH values. Thereafter, the elastomers were tested for cell viability using human neuroblastoma cells (SH-Sy5Y) and human myoblasts cells (C2C12). These two cell lines were chosen as examples for tissues in the human body (SH-Sy5Y as cancer cells and C2C12 as skeletal muscle cells representing the potential use of our scaffolds for *in vitro* studies of cancer cells and tissue regeneration using muscle cells). Ultimately, the exceptional properties imparted by the liquid crystalline nature of the poly(ε-caprolactone)-based LCEs are hoped to trigger on-demand ordering and alignment that can be manipulated using substrates (commonly used for alignment of LC molecules in display devices), applied fields, or mechanical deformation (stretching, twisting), or in the near future steer direct differentiation of stem cells, control cell adhesion and growth rate, and potentially allow for simultaneous incorporation of oriented vascular networks, for example, by co-culturing of endothelial cells.[4]

2. Results and Discussions

2.1. Synthesis of Star Block Copolymers and Elastomers

The synthesis of functional LCEs for the preparation of smart responsive scaffolds (SRS) materials in this report is based on SBCs with glycerol as central node, from which

arms of random blocks of ε-caprolactone-, halogen-substituted ε-caprolactone- (α- or γ-substituted) and (D,L)-lactide-based polyester units extent (Scheme 1). The synthesis follows a modified procedure previously reported by Younes et al.[17] In a quasi solvent-free melt-polymerization at 140 °C, the hydrophobicity is to some degree tunable, which is critical for cell attachment (vide infra). The hydrophobicity is controlled by the initial ratio of the building blocks ($x + y$:$z = 1$:1), with the two ε-caprolactone-based moieties (blocks x and y) being slightly more hydrophobic than the (D,L)-lactide segment (block z).[20] **SBC-αCl** and **SBC-γBr** were characterized using FT-IR (Figure S1), ^{1}H NMR, DSC, TGA and gel permeation chromatography (GPC). In designing these SBCs, the molar ratio of the halogen atom modified ε-CL block at the α- or γ-carbon with respect to unmodified ε-CL can easily be adjusted from 0 to 100 mol-% of the final elastomer with one extreme providing a non-LC elastomer and the other extreme a LCE with each caprolactone monomer carrying a cholesterol group. After the first syntheses clarified that the 5 mol-% was not liquid crystalline and the 40 mol-% to mechanically tough for cell growth and cell penetration, we decided to focus on a narrower window of opportunity, and present here the data for two specific compositions that show, as we will see later, rather similar mechanical properties. For the α-position LC-modified LCE (**LCE-α**) we chose the composition where 10% (every tenth CL molecule) of the ε-CL monomers are functionalized with cholesterol, and for the γ-position modified LCE (**LCE-γ**) the composition where 15% (every seventh CL molecule) of the ε-CL monomers carry the CLC pendant group. These ratios are highlighted in Scheme 1, but in the text we will refer to them only as **SBC-α** (or **SBC-γ**) and **LCE-α** (or **LCE-γ**). The increased molecular flexibility of the LC pendant groups in the γ position (not right next to the carbonyl group in the α position) appears to lead to final LCEs with rather similar tensile properties at least at lower stresses but a different internal morphology as discussed later. The composition of the products was determined and found to be close to the hypothetical value for the starting molar ratios in the synthesis as determined by ^{1}H NMR of the **SBC-αCl** and **SBC-γBr**. Existence and transformation of functional groups was tested by FT-IR spectroscopy. Here, the FT-IR spectra of both **SBC-αCl** and **SBC-γBr** are shown in Figure S1. After substitution of the halogen atoms with azide groups, the expected azide band appears at around 2 100 cm^{-1}. The success of this displacement reaction was also confirmed by a higher chemical shift observed of the α (or γ) proton in the ^{1}H NMR spectra of **SBC-αN$_3$** and **SBC-γN$_3$** compared to **SBC-αCl** and **SBC-γBr**. The products of the "click" reactions with **1**, **SBC-αCLC** and **SBC-γCLC**, were also analyzed by FT-IR, where as expected, the azide band at 2 100 cm^{-1} disappeared completely and a new band at 3 020 cm^{-1} appeared indicative of an aromatic hydrogen resulting from the formation of the heterocyclic triazole ring (Figure S1). The formation of the triazole ring is also confirmed by the presence of a singlet observed at around 7.33 ppm in the ^{1}H NMR spectra. GPC was used to determine the molecular weight of the star block co-polymers. Table S1 (SI) details the molecular weight distribution and polydispersity indices (PDI) of these SBCs before the cross-linking step.[21] The synthesis delivers SBCs with the desired low molecular weight (lower molecular weight facilitates faster biodegradation rates) with realistic polydispersity indices (PDI $= \overline{M}_w/\overline{M}_n$) and a unimodal peak in gel permeation chromatography (GPC). It has been reported that low monomer concentration (provided by melt rather than solution polymerization) reduces the polymerization rate and increases the chance of chain termination and irreversible reactions that result in more heterogeneous polymers with somewhat higher PDI.[21]

A cross-linking step then produces the elastomers with pendant cholesterol-based LC moieties, which would be regarded as side-chain LCEs, however, not exclusively composed of reactive LC units (Scheme 2). As we will see, however, even this rather low degree of liquid crystal functionalization leads to LCEs composed of biocompatible and in principle FDA-approved components that can be used as a 3D cell scaffold, which represents an entirely new, not heretofore reported area of application for LCEs.

2.2. Mesomorphic and Thermal Characterization

The mesomorphic properties of cholesteryl 5-hexynoate (**5**), the cholesterol-modified **SBC-*x*CLC** ($x = \alpha$ or γ) polymers, and the final cross-linked LC-functionalized elastomers (**LCE-α** and **LCE-γ**) were investigated by POM (Figure 1), DSC and SAXD. The cholesteryl 5-hexynoate **1** showed two liquid crystal phases, a smectic-A (SmA) and a chiral nematic (N*) phase. The polarizing optical microscopy showed a typical oily streak texture (Figure 1A) for the N* phase and a pseudo fan shape texture often observed for a SmA phase (Figure 1B) on cooling with a phase sequence of Cr 55.3 SmA 71.9 N* 76.3 Iso (°C). **SBC-αCLC** (Figure 1C) and **SBC-γCLC** (Figure 1D) showed fan shaped textures indicative of a SmA phase. As expected for polymers with slightly larger PDI, the co-polymers **SBC-αCLC** and **SBC-γCLC** showed broad phase transitions both in POM and DSC experiments, but exhibit the smectic-A phase up to about 70 °C, i.e., the liquid crystal phase exists well below and well above room temperature, which translates to the final cross-linked elastomers.

DSC data confirmed that both SBCs were semi-crystalline in nature with T_gs well below physiological temperatures. As expected, the glass transition temperatures increased after cross-linking.[15] The final elastomers appeared amorphous with no endothermic peaks indicative of melting, and also showed T_g values significantly below

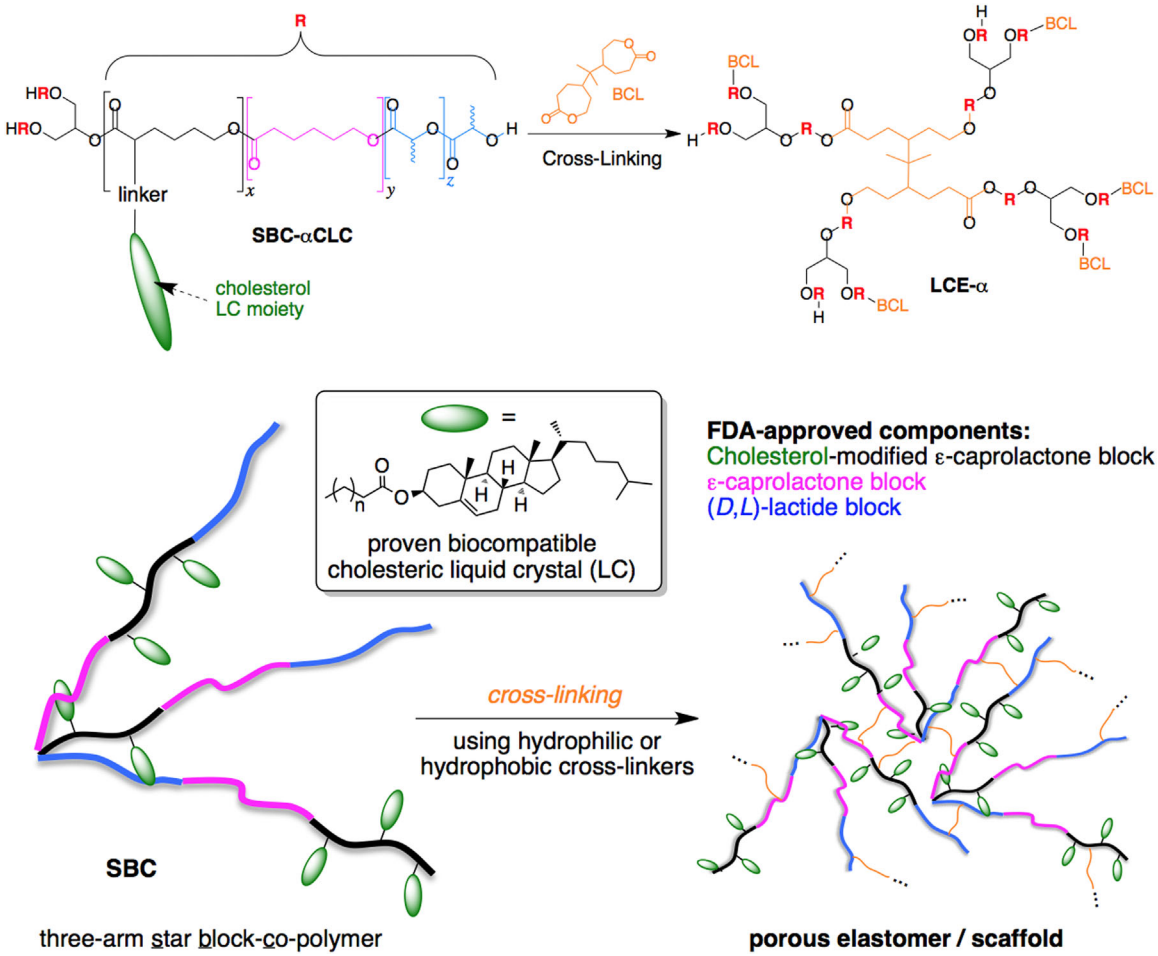

Scheme 2. Crosslinking with bis-caprolactone (BCL) results in the formation of LCEs with pendant cholesteric LC groups (α position shown). A simplified schematic shows the random nature of the SBCs and the crosslinking in the final elastomer.

physiological temperatures. A summary of all glass transition temperatures determined by DSC and decomposition temperatures (ranging from 190 to 260 °C) measured by TGA is given in Table 1.

Thermal gravimetric analyses (Figure S2) of the block copolymers show that the replacement of a halogen in the **SBC-*x*Cl**(**Br**) with a bulkier group, such as cholesterol, results in less volatile co-polymers. Also, an increase in decomposition temperature by ≈45 °C is observed in all block copolymers with cholesterol pendant groups (**SBC-αCLC** and **SBC-γCLC**) when compared with block copolymers featuring halogen (**SBC-αCl** and **SBC-γBr**, see Table 1), and the overall thermal stability increases to about 200 °C. While the elastomers are too viscous to obtain very homogeneous thin-film POM textures to assign phase transition temperatures (Figure 1E and F), SAXD allowed us to make a clear phase assignment.

The 2D SAXD pattern and intensity profiles of liquid crystal functionalized **SBC-*x*CLC** co-polymers and final LC elastomers (**LCE-*x***) at a representative temperature of 50 °C are shown in Figure 2. All SAXD pattern clearly show two scattering maxima with $q_1{:}q_2 = 1{:}2$ ([100] and [200]) in the medium angle region indicating an ordered layer structure. and a broad wide-angle peak (halo) at a scattering vector typical for the distance between molten hydrocarbon chains. Table 2 summarizes the X-ray diffraction data at this temperature. The length of side chain cholesterol pendant group with six methylene groups and the triazole heterocyclic structure from the "click" reaction was calculated to be $l = 3.3$ nm by simple MM2 energy minimization in 3D-Chemdraw 13.0. The calculated d-spacing (ranging from 4.0 to about 4.1 nm) for **SBC-αCLC**, **SBC-γCLC**, **LCE-α**, and **LCE-γ**, correspond well to an almost fully interdigitated (bilayer-type) arrangement with a side-by-side packing of the cholesterol cores, indicating that the liquid crystal phase should in all cases be regarded as an interdigitated smectic-A phase (SmA). SAXD data for the LCEs always show very similar scattering patterns and d-spacing values in comparison to the parent SBC but with lower intensities, which is attributed to the amorphous

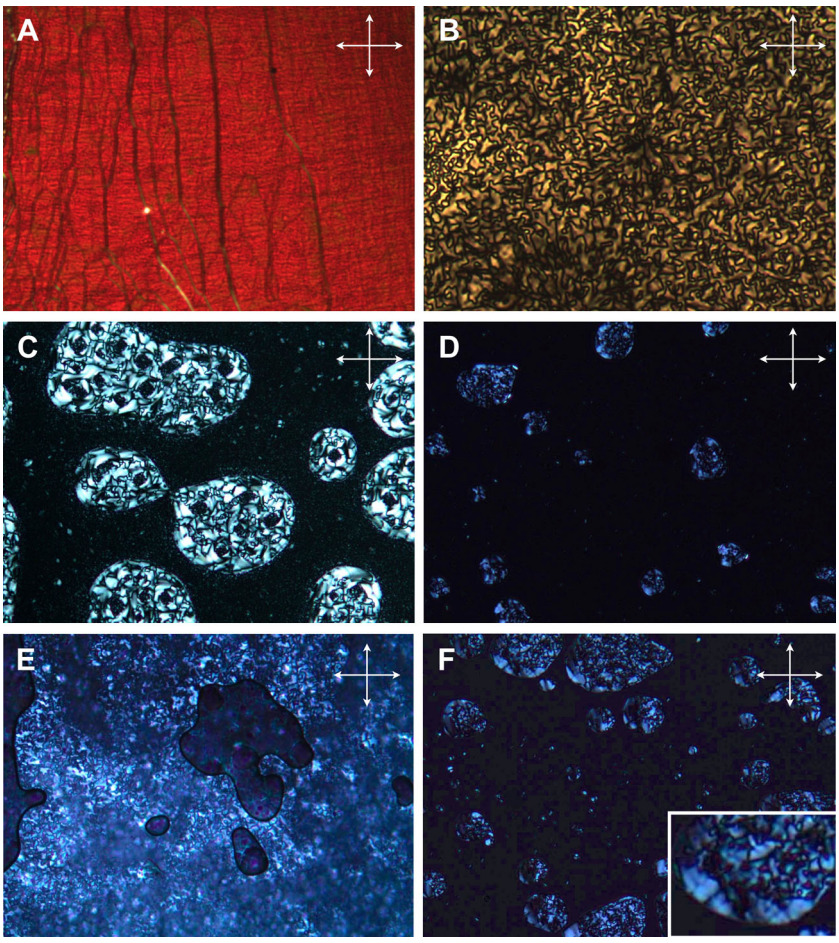

Figure 1. Polarized optical photomicrographs (crossed polarizers) as observed on cooling of: (A) the N* of **1** at 71.6 °C, (B) the SmA phase of **1** at 70 °C, (C) the SmA phase of **SBC-αCLC** at 50.7 °C, (D) the SmA phase of **LCE-α** at 40.0 °C, (E) the SmA phase of **SBC-γCLC** at 52.3 °C, and (F) the SmA phase of **LCE-γ** at 41.0 °C.

Table 1. Thermal Analysis of polymers and elastomers.

Material	DSC	POM	TGA
	T_g [°C]	"Isotropic"[a)] [°C]	$T_{decomp.}$ [°C]
SBC-αCl	−39.2	–	201.8
SBC-αCLC	−21.6	73.5	245.8
LCE-α	−37.2	72.1	260.2
SBC-γBr	−26.2	–	189.3
SBC-γCLC	−37.1	60.0	235.1
LCE-γ	−22.1	73.0	252.3

[a)]"Isotropic" for LC elastomers refers to "melting of partially crystalline polymer" or softening point of the polymers. [abbreviations: DSC = differential scanning calorimetry, POM = polarized optical microscopy, TGA = Thermogravimetric analysis].

nature of the elastomers. Similar liquid crystal phase behavior of cholesterol-based LC elastomers has previously been reported for side chain liquid crystalline functionalized block copolymers, homopolymers[22–25] and liquid crystalline brush block copolymers.[26] Figure S3 shows the temperature dependent SAXD of **SBC-*x*CLC** polymers and **LCE-*x*** elastomers. Upon approaching temperatures closer to SmA-Iso phase transition (at ≈70 °C) the intensities of the diffraction peaks decrease continuously and considerably close to the phase transition, and show a trend of decreasing *d*-spacing values with increasing temperature. The model in Figure 2c representatively shows the proposed organization of the cholesterol pendants in both the SBCs and the final LCEs.

2.3. Morphological Characterization

A critical feature for the proposed use of the LCEs for 3D cell culture studies using scaffolds is the internal morphology of the elastomer materials. The **SBC-*x*CLCs** after cross-linking with BCP are reasonably mechanically tough side-chain LCEs. **LCE-α** appears to be the more rough, yet highly porous elastomer, however with an overall lower pore density, whereas **LCE-γ** features a higher pore density and much more homogeneous pores (similar to Swiss cheese) with an average pore size of about 5 μm (see Figure 3). Critically, both elastomers feature pore sizes suitable for "housing" cells once the elastomers are swollen in cell culture media. The difference in internal morphology highlights that the position of the cholesterol groups along the ε-CL backbone segments is important, and that either a higher molecular flexibility of the cholesterol groups at the γ-position or a higher degree of LC-functionalization (15% vs. 10%) in the ε-CL blocks leads to LCEs with a higher pore density and more homogeneous internal morphology. Since all LCE-γ compositions (ranging from 10 to 40 mol-%) show higher pore densities in SEM images, the former appears to be the relevant parameter affecting porosity in these materials (see Figure S5 in SI). All samples used for SEM were obtained from disks (Ø = 2 cm) from ampoules (serving as a mold during crosslinking) after careful microtoming to obtain 60, 100, or 200 μm thick slices that were also used for cell culturing and subsequent confocal microscopy studies.

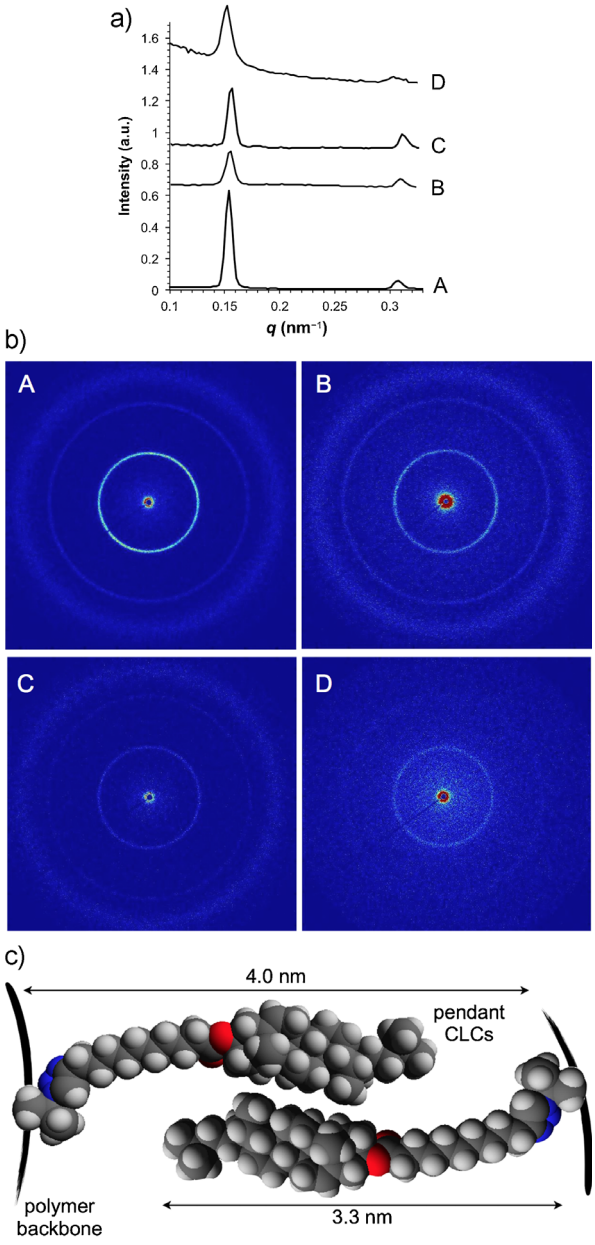

Figure 2. (a) Azimuthally averaged intensity data of the scattering vector (q) vs. intensity of 2D SAXD pattern in (A) **SBC-αCLC**, (B) **LCE-α**, (C) **SBC-γCLC**, and (D) **LCE-γ** all at 50 °C, (b) 2D small and mid-angle X-ray diffraction patterns (for A–D, see (a); the broad diffuse scattering particularly visible in A-C is from the Kapton® windows. (c) Model of the molecular arrangement of the pendant cholesteric LC groups leading to the formation of smectic-A SBCs and LCEs. A side-by-side packing of the cholesteric cores as shown in the cartoon matches the experimentally observed layer spacing of around 4 nm.

2.4. Tensile Studies

The viscoelastic properties of the three elastomers samples (**LCE-α, LCE-γ**, and the unmodified elastomer) were measured using a Linkam tensile stage (see Experimental Section). As can be seen in Figure 4, the unmodified non-LC elastomer shows the least resistance to mechanical deformation, which as we found earlier does depend on the cross-linking density.[17] At the same cross-linking density used for the current unmodified elastomer sample, both **LCE-α** and **LCE-γ** are more resistant to strain, which can only be explained by the presence of the liquid crystalline character of these two LCEs. **LCE-α** initially shows a logarithmic increase in stress followed by a more or less linear increase until it breaks well above the 20% strain shown in Figure 4. **LCE-γ** shows the same initial logarithmic slope up to about 4%, which is the regime suitable for potential effects on cells. Thereafter, however, **LCE-γ** shows a sudden increase, which we attribute to a disorder-order transition of the pendant CLC moieties due to the higher mol% of CLC substitution in **LCE-γ**. This ordering event might well be associated to the increased molecular flexibility of the CLC pendants in the γ-position of the ε-CL blocks in **LCE-γ**, as well as the presence of pores that can interrupt the bulk response of the elastomer in response to strain (pores deform). Apart from this, both **LCE-α** and **LCE-γ** show rather similar values and slopes up to strain values of 10%. The values for Young's modulus (E in MPa; calculated following the approach outlined by Ratna and coworkers[27]) and the ultimate strain (ε in %) are shown in Figure 4 near to each data set as well.

Table 2. Measured scattering vectors (q in Å^{-1}) with respective Miller indices, and calculated d spacing in nm at 50 °C.

Material	$q_{(hkl)}$ [nm]$^{-1}$	d [nm]
SBC-αCLC	$q_{(001)} = 0.154$	4.08
	$q_{(002)} = 0.305$	
LCE-α	$q_{(001)} = 0.153$	4.10
	$q_{(002)} = 0.305$	
SBC-γCLC	$q_{(001)} = 0.158$	3.98
	$q_{(002)} = 0.313$	
LCE-γ	$q_{(001)} = 0.154$	4.08
	$q_{(002)} = 0.303$	

2.5. Degradation Studies

To demonstrate the biodegradable nature of these LCEs and determine the degradation rates, we performed biodegradability studies using **LCE-α** as a characteristic sample and compared the rate with a sample of the unmodified elastomer at identical conditions. To do so, we subjected two slab specimens (to ensure reproducible results) of both elastomers to *in vitro* degradation in PBS buffer at different pH values (3, 7, and 11). In a standard

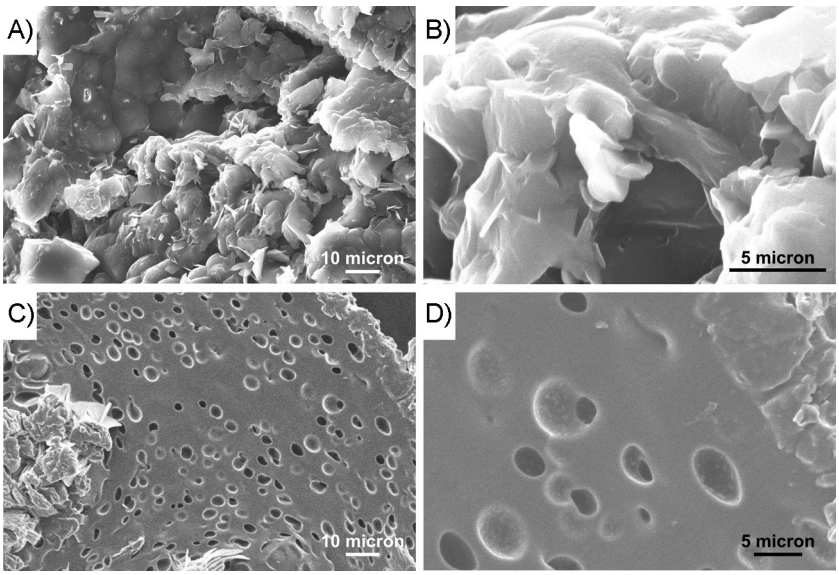

Figure 3. SEM images showing the internal morphology of: (A and B) **LCE-γ** (cross-sectional view) and (C and D) **LCE-γ**, (cross-sectional views; 5 μm average pore size).

procedure, samples were examined by weighing for a period of 15 weeks. Figure 5 shows the % weight change of the samples as a function of time. Both samples at all pH values experienced the main increase of weight in the first week due to water absorption (swelling). For every weight gain thereafter, an increase in weight is attributed to water absorption from the degradation media into the slabs' bulk. The diffusion of water into caprolactone-lactide elastomers at temperatures above T_g decreases as the cross-linking density of the elastomer increases.[17] Caprolactone-lactide co-polymers are known to degrade primarily *via* bulk acid-catalyzed hydrolysis. The degradation is auto-catalyzed because the hydrolysis reaction produces oligocarboxylic acids and is anticipated to start at the cross-linking sites. The weight initially and throughout the degradation studies increased periodically due to the formation of degradation products within the matrix that enhance the degradation and draw water into the polymer matrix *via* osmosis, and of the resulting degradation products leach out of the elastomer slab. In effect, each time the specimen experienced a major degradation process; the weight of the specimen increases right after due to the osmotic draw of water from the aqueous or buffer solution. At the end of week 15, neither of the elastomer samples had degraded completely. Both samples had become very paste-like with a much less definable form (Figure S6, SI). Each sample degrades, as expected more rapidly in acidic and basic medium (at pH 3 and 11), and substantially slower in the neutral buffer (PBS) as can be seen by major weight gains and losses in comparison to the PBS buffer medium. Since we use ethanol to sterilize the elastomers 10 min at a time, all specimens were also tested in ethanol, where the elastomers survived for more than the sufficient timeframe of about 5 weeks. As a major outcome of these test, the LC modified **LCE-α** degrades faster, showing that the biodegradation rate is affected by LC modification in the polymer backbone. Critically, **LCE-α** survives for at least 10 weeks before major biodegradation sets in, long enough to allow in principle for generation of tissue if these LCEs were used as a cell scaffold.

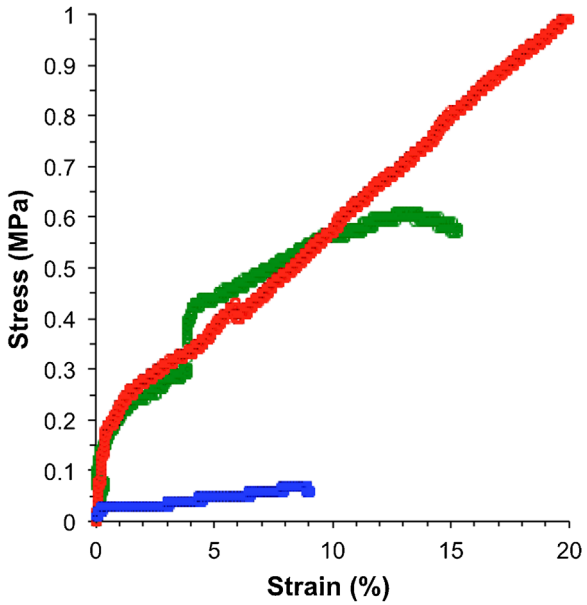

Figure 4. Strain–stress curves of **LCE-α** (red data points), **LCE-γ** (green data points), and unmodified elastomer (blue curve). Both the unmodified elastomer and **LCE-γ** break at lower applied strains (9 and 15%, respectively) in comparison to **LCE-α**. The ultimate strain (ε in %) and the Young's modulus, E in MPa (calculated from the initial slope at small stress values) are next to each graph for all three elastomers.

2.6. *In Vitro* Cell Biocompatibility Studies

To determine the viability of cells on and within the LC elastomers we tested the viability of two distinct cell lines, neuroblastomas (SH-Sy5Y) and myoblasts (C2C12). It is well known that some types of cells adhere to more hydrophilic surfaces,[28] whereas other types of cells prefer more hydrophobic environments. Before incubating C2C12, a representative slice of **LCE-α** was also exposed to O_2 plasma (routinely used to sterilize materials) known to affect not only the surface morphology but also the surface chemistry

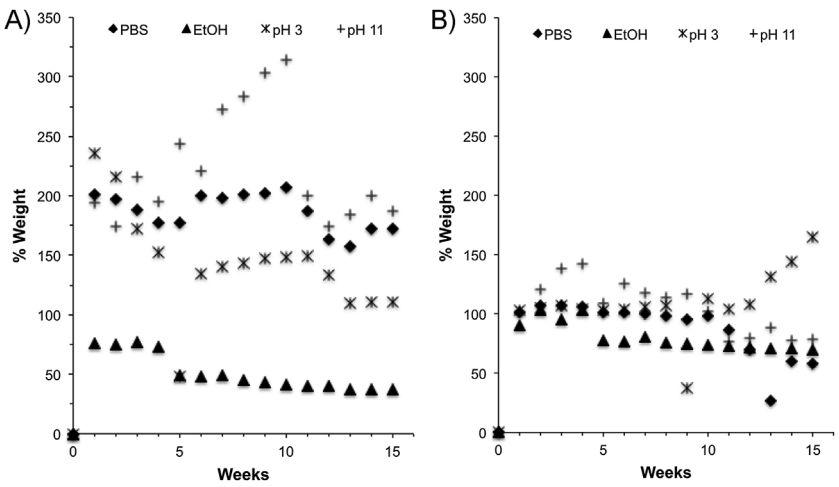

Figure 5. Biodegradation plots (time vs. % weight change) for: (A) **LCE-α** and (B) unmodified elastomer. Plots for each specimen in each medium were identical for both samples for each specimen (tested by two experimenters each).

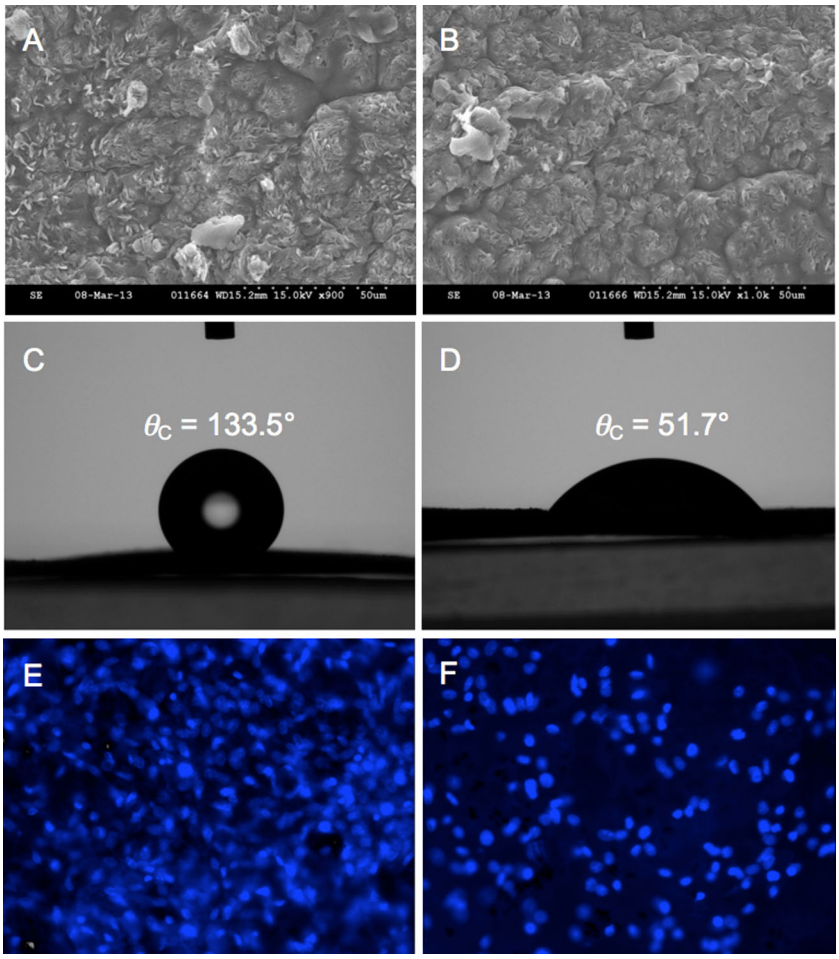

Figure 6. SEM images of **LCE-α** (A) before and (B) after exposure to O_2 plasma, contact angle measurement before (C) and after (D) O_2 plasma sterilization, and (E) and (F) human myoblasts (C2C12) cells incubated on **LCE-α** before and after O_2 plasma sterilization (cell nuclei are visible after ToPro® staining).

(formation of hydrophilic functional groups such as hydroxyl [—OH] and hydroperoxyl [—OOH]) groups in polyesters, which is accompanied by surface degradation.[29] The smaller roughness features on the surface of the O_2 plasma treated **LCE-α** are clearly discernable by SEM (see Figure S4, SI). Contact angle measurements confirmed the difference in hydrophobicity between the O_2 plasma-exposed and un-exposed (control) **LCE-α** sample (Figure 6). C2C12 were then seeded and incubated at 37 °C and 5% CO_2 for 24 h. Thereafter, the LC elastomers were examined and cell confluence was studied using confocal microscopy (Figure 6). The O_2-plasma exposed **LCE-α** showed a decrease of hydrophobicity on the surface, which resulted in a low density of C2C12 cells on and within the porous 3D **LCE-α** network. On the contrary, the un-exposed control **LCE-α** showed remarkably high cell density on and throughout the **LCE-α** 3D pore network, as anticipated for C2C12 cells preferring a more hydrophobic environment for growth and expansion. However, cells preferring a more hydrophilic environment would be experience a better 3D microenvironment in the plasma treated elastomer.

In the case of the SH-Sy5Y, known to prefer a more hydrophilic environment, the cells were seeded on the **LCE-γ** elastomers and incubated at 37 °C and 5% CO_2 for 24 h as well. After 2 and 7 d of incubation, the LC elastomers were examined and the cell confluence was studied using confocal microscopy (Figure 7a, A–F). SH-Sy5Y cells clearly appeared to attach, grow, and proliferate on and within the elastomer, however the density appeared lower than in the case of the myoblasts discussed earlier. To increase the density of cells growing on the elastomer, sets of **LCE-γ** samples were divided into three groups; control (untreated elastomer), elastomer dipped in D-lysine and elastomer dipped in collagen. SH-Sy5Y were then seeded separately on top of the three sets of elastomers and incubated at 37 °C and 5% CO_2 for 24 h. After incubating the seeded elastomers for about 2 d, cell confluence

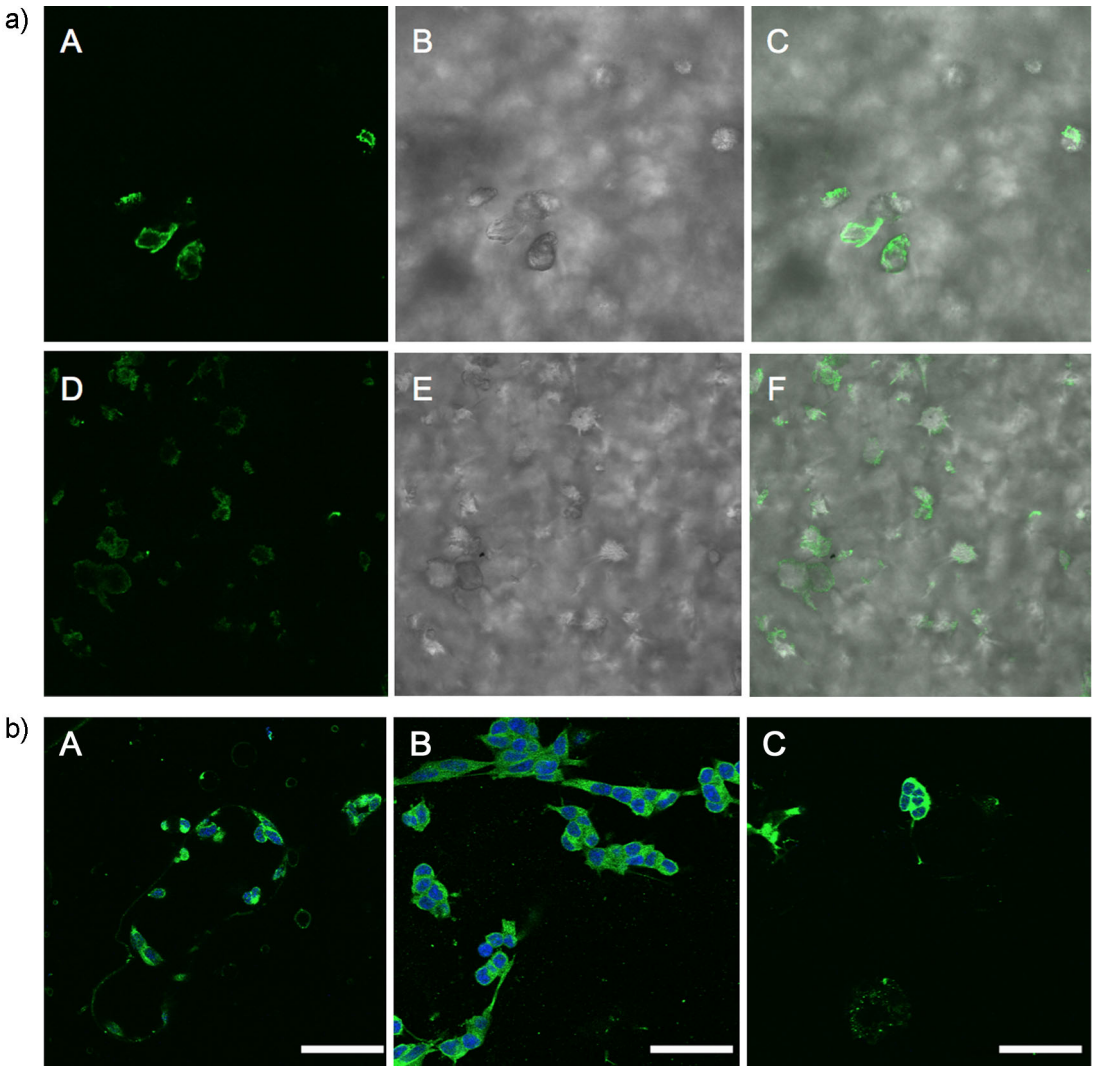

Figure 7. (a) Fluorescence confocal microscope images of human neuroblastoma cells (SH-Sy5Y) cultured in **LCE-γ** using DMEM as cell culture medium: (A–C) for 2 d, (D–F) for 7 d prior to fixing and staining with DIOC6 (fluorescence, bright field, and combined channels from left (A, D) to right C, F)). Note the increased cell count after 7 d indicating that the cells thrive within **LCE-γ**. (b) Fluorescence confocal images comparing **LCE-γ** in: (A) the natural state, (B) coated with collagen, and (C) coated with D-lysine prior to staining with DIOC6 (green) or nuclear stain (blue). Scale bars (50 μm) are representative for each column of images.

data as confirmed by confocal microscopy showed that SH-Sy5Y seeded on collagen-dipped **LCE-γ** showed the highest cell density followed by the untreated control and finally the lowest cell density for the D-lysine-dipped **LCE-γ** (Figure 7b). Treating **LCE-γ** with a collagen solution appears to fill the pores of the elastomer with collagen, creating a temporary hydrophilic environment that allowed the cells to attach and proliferate despite the more hydrophobic environment of the native LC elastomer. Giving time to the cells to create their own extracellular matrix (ECM) and temporarily providing a more suitable, hydrophilic environment for proliferation within the 3D elastomer network allowed the cells to thrive in the LC elastomer. SH-Sy5Y cells were also seeded on parent elastomers samples not modified with cholesterol. While cells attached and proliferated, significantly lower cell densities were observed in comparison to the liquid crystal modified elastomer samples such as **LCE-γ** without collagen (Figure 7a). One significant reason for this behavior is that the addition of a LC moiety renders this type of elastomer softer than the non-LC modified, parent elastomer prepared under the exact identical reaction conditions.

3. Conclusion

We here presented a modular, solvent-free synthesis of biodegradable and biocompatible smectic LCEs with tunable porosity. For the first time, LCEs have been

successfully used as 3D cell culture scaffolds. The straightforward synthesis determines the mechanical properties (stiffness, flexibility, porosity), which in turn adjusts cell adhesion onto and into these hydrophobic elastomers. Tunable hydrophilicity and hence water contact angle via O_2 plasma etching was found to be a very useful, highly relevant approach for cell seeding while avoiding an additional Matrigel™ layer (usually applied by dipping, drop-casting or spin-coating), needed previously in experiments described by others,[30a] that in turn would mask the surface ordering of the LCEs.

Using DSC, POM, and SAXD analysis we confirmed that both the **SBC-*x*CLC**s and the final **LCE-*x*** elastomers functionalized with cholesterol pendants exhibit smectic-A phases over a wide temperature range including room temperature. Thus all cell studies; especially the cell seeding, were carried out with the LCE scaffolds in the smectic-A phase.

The position of the liquid crystal functionalization (α vs. γ) is easily controlled by the choice of starting monomers, and affects both thermal and macroscopic properties such as the porosity and tensile properties of the LC elastomers. Abbott and co-workers[30] demonstrated the interplay between liquid crystal ordering and stem cell attachment and proliferation on Matrigel™-covered liquid crystal-stem cell interfaces, and these experiments served as a guide for the choice of the LC pendant group described here.

Another critical point of the overall design is the degree of cross-linking in the final LCE that can be controlled by the amount of cross-linker (bis-ε-caprolactone, orange in Scheme 1) added to the SBCs in the final step or by choosing central nodes with more than three arms. The degree of cross-linking can and will be used in future work to tune not only the thermal and mechanical properties of these LC elastomers, but also the porosity, which will allow for integration (by swelling and soaking up) of collagen or any other desirable substances needed for specific tissue culture such as growth factors for 3D cell culturing of a variety of cells.

Ongoing experiments now focus on investigating the type of cross-linker and overall number and density of the liquid crystal pendant groups (up to 40% by weight) on the porosity, elastic properties as well as cell adhesion and proliferation on and within these LC elastomers. In addition, long-term studies will focus on cell response to external stress to the LCE elastomer scaffolds.

4. Experimental Section

4.1. Materials

All air sensitive manipulations were carried out under nitrogen gas; ε-caprolactone (ε-CL, Alpha Aesar) was dried over calcium hydride and distilled under reduced pressure. Stannous 2-ethylhexanoate, glycerol, and triethylamine were used as received (Sigma–Aldrich). 3-chloroperbenzoic acid (*m*-CPBA) was dissolved in diethyl ether and the ether solution in a separation funnel was washed with a buffer solution (prepared from 1.28 g sodium phosphate monobasic monohydrate and 8.24 g sodium phosphate dibasic heptahydrate in 800 mL distilled water and adjusted pH at 7.4). The aqueous and organic phases were separated and the organic phase was dried with sodium sulfate (2–4 g of drying agent is directly added to the ether solution) before use. Diethyl ether, dichloromethane, and dimethylformamide (DMF) were dried by passage through an activated alumina column (solvent purification system (Innovative Technology, PureSolv MD5 solvent purification system). Tetrahydrofuran (THF) was dried over a benzophenone-sodium mixture and distilled under nitrogen. Toluene was dried over 4 Å activated molecular sieves. Methanol (Alpha Aesar), ethanol (Alpha Aesar), D,L-Lactide (D,L-LA, Alpha Aesar), chromium(VI) oxide (Sigma–Aldrich), pyridinium chlorochromate (Sigma–Aldrich), sodium sulfate (Sigma–Aldrich), sodium bicarbonate (Sigma–Aldrich), and sodium thiosulfate (Fisher Scientific) were used as received. Hyclone cell media (DMEM) and Trypsin (0.25% content) were purchased from VWR Scientific and used as received. Fetal bovine serum (FBS) and penicillin/streptomycin were purchased from Fisher Scientific and used as received. Both human myoblast (C2C12) and human neuroblastoma (SH-Sy5Y) cell lines were purchased from American Type Culture Collection (ATCC).

4.1.1. Glass Silanization

All glass ampoules and glass slides used for the preparation of star-block copolymers and elastomers were previously silanized using a 2% (v/v) solution of Me_3SiCl in acetone. Ampoules are filled with the silanizing solution and stirred for about 4 h, then rinsed with acetone and dried in an oven at 140 °C. Glass slides were immersed in the silanizing solution and stirred for 4 h, then rinsed with acetone and dried in an oven at 140 °C.

4.1.2. Substrate Cleaning and Plasma Treatment

Once coverslips were cleaned by piranha solution (mixture of 98% H_2SO_4 and 30% H_2O_2 with v/v = 7:3) for 20 min, they were thoroughly washed with Milli-Q water (18.2 MΩ · cm) and dried under a nitrogen stream. The cleaned substrates were then exposed to oxygen plasma in an oxygen plasma cleaner (PDC-32G, Harrick Plasma, Ithaca, NY) with a power of 18 W for 2 min. The oxygen plasma breaks down weak surface bonds and replaces them with highly reactive hydroxyl groups. Elastomers were cleaned with 70% ethanol, rinsed with Milli-Q water (18.2 MΩ · cm), dried under a nitrogen stream and then exposed to oxygen plasma with a power of 18 W also for 2 min.

4.2. Synthesis

4.2.1. Synthesis of Monomers and Reaction Intermediates

All compounds were synthesized according to previously reported methods. Details for the elastomers with 5 mol-% of modified ε-CL block are provided below. All other experimental details and ^1H NMR

spectra of reaction intermediates to the halogen-substituted ε-CLs, the biscaprolactone (BCL) cross-linker, and the liquid crystal pendant precursor (**1**) are given in the supplementary information (SI).

4.2.2. Synthesis of α-Cl-three Arm Star Block Copolymer: Poly(ε-CL-co-α-Cl-ε-CL-co-D,L-LA), (SBC-αCl)

The general procedure for the synthesis of SBC of ε-CL and (D,L)-LA, developed by Amsden and coworkes,[17] was used and slightly modified as follows: In a dry, silanized ampoule, glycerol (2.5 μL, 0.033 mmol) was mixed with ε-CL (3.64 g, 33 mmol) and α-Cl-ε-CL (0.5 g, 3.3 mmol) and mixed using a vortex mixer for about a minute, then (D,L)-LA (7.2 g, 50 mmol) was added. The solution was mixed again using the vortex mixer, the ampoule was purged with nitrogen and placed in the oven at 120 °C until melting of (D,L)-LA. The contents were then again mixed on a vortex mixer and tin(II) 2-ethylhexanoate (66 μL, 0.20 mmol) was added and mixed one last time. The ampoule was again flushed with nitrogen, flame-sealed under vacuum, and placed in a sand bath for 48 h at 140 °C. The ampoule was then removed from the sand bath, the seal was then broken and the highly viscous liquid was dissolved in dichloromethane. The obtained solution was then poured into cold methanol (cooled using a dry ice/acetone bath at a temperature around −78 °C). A white precipitate was obtained and was removed by filtration. The filtrate was dried in a vacuum oven at 50 °C. The purified product was characterized using ^{1}H NMR, FT-IR, DSC, and TGA. ^{1}H NMR ($CDCl_3$, 400 MHz) δ[ppm]: 5.3–5.02 (m, COC*H*CH_3), 4.4–4.28 (m, C*H*Cl), 4.23–4.11 (m, CH_2O), 4.10–4.04 (t, $J = 4.6$ Hz, CH_2O), 3.75–3.65 (m, C*H*CH_2), 3.10–2.62 (broad, s, OH), 2.39 (t, $J = 4.5$ Hz, α–H), 2.32 (t, $J = 5.1$ Hz, α−H), 1.82–1.2 (m, CH_2, CH_3). ^{13}C NMR ($CDCl_3$, 100 MHz): δ 173.63, 172.91, 170.91, 69.35, 66.70, 65.33, 64.17, 34.10, 28.28, 25.30, 24.55, 20.39, 16.94. FT-IR (KBr) 1/λ [cm^{-1}]: 2 932 (s), 2 860 (m), 1 720 (s), 975 (s), 884, 787 (m). Glass transition temperature (T_g) was found at −39.2 °C, and decomposition temperature at 201.8 °C.

4.2.3. Synthesis of γ-Br-three arm SBC: star-poly(ε-CL-co-γ-Br-ε-CL-co-DL-LA), (SBC-γBr)

A dry silanized ampoule was filled with (D,L)-LA (7.2 g, 50 mmol), ε-CL (4.85 g, 42 mmol), and γ-Br-ε-CL (1.16 g, 6.0 mmol). The ampoule was placed in an oven at 120 °C until (D,L)-LA melted. Once (D,L)-LA has melted the ampoule was placed on mixed a vortex fro about a minute. Glycerol (0.36 mL, 5.0 mmol) and tin(II) 2-ethylhexanoate as catalyst (0.04 mL, 0.10 mmol) were added to the ampoule. The ampoule was purged with nitrogen, and its contents were mixed one more time using vortex mixer, and flame-sealed under vacuum. The ampoule was finally placed in a sand bath at 140 °C for 24 h. The resulting star block copolymer (**SBC-γBr**) was purified by precipitation from dichloromethane solution into a methanol solution cooled using dry ice and acetone mixture (at –78 °C). The purified product was characterized using ^{1}H NMR, FT-IR, DSC, and TGA. ^{1}H NMR ($CDCl_3$, 400 MHz), δ[ppm]: 5.13 (m, COC*H*CH_3), 4.18–4.09 (m, CH_2O), 4.12 (t, $J = 4.5$ Hz, CH_2O), 4.05 (t, $J = 4.4$ Hz, CH_2O), 3.75–3.65 (m, C*H*CH_2), 3.62 (m, C*H*Br), 3.14 (broad, s, OH), 2.38 (t, $J = 4.7$ Hz, α-H), 2.29 (t, $J = 4.7$ Hz, α′-H), 1.70–1.30 (m, CH_2, CH_3). FT-IR (KBr) 1/λ [cm^{-1}]: 2 930 (s), 2 860 (m), 1 720 (s), 1 450 (s), 959 (m), 864 (m), 741 (m). Glass transition temperature (T_g) was found at −26.2 °C and its decomposition temperature at 189.3 °C.

4.2.4. Synthetic Modification of α-Cl-Three Arm SBC to α-N_3-Three Arm SBC: Poly(ε-CL-co-α-N_3-ε-CL-co-DL-LA), (SBC-αN_3)

In a round bottom flask, SBC-αCl (5 g, 3.36 mmol) was dissolved in dry dimethylformamide (DMF) under nitrogen. Then 0.22 g of sodium azide (NaN_3 3.38 mmol) was added and the contents were allowed to react overnight at room temperature. DMF was removed under reduced pressure and the remaining mixture was dissolved in toluene. The solution was then centrifuged (5 000 rpm for 15 min) thrice to remove the salt formed. Toluene was then evaporated under reduced pressure. The final purified product was characterized using ^{1}H NMR and FT-IR. ^{1}H NMR ($CDCl_3$, 400 MHz) spectrum was similar to the parent SBC-αCl with the exception of the appearance of a peak at 3.89 ppm related to the azide group. The azide-SBC_1 (SBC-αN_3) characterized by FT-IR was compared against the parent SBC-αCl which confirmed the presence of a peak at 2 100 cm^{-1} related to the azide stretch (KBr, 1/λ [cm^{-1}]): 2 930, 2 100 (s, azide), 1 720 (s), 1 450 (s), 954 (m), 861 (s), 733 (s), 696 (m). ^{13}C NMR (CDCl3, 100 MHz): δ 175.10, 173.70, 172.97, 170.33, 169.61, 69.35, 68.22, 66.71, 65.32, 64.20, 34.10, 33.66, 28.29, 25.49, 24.54, 16.74.

4.2.5. Synthetic Modification of γ-Br-Three Arm SBC to γ-N_3-Three Arm SBC: Poly(ε-CL-co-γ-N_3-ε-CL-co-DL-LA), (SBC-γN_3)

In a round bottom flask, 1.5 g of **SBC-γBr** (0.60 mmol) was dissolved in 15 mL dry DMF. Then 0.045 g of NaN_3 (0.60 mmol) was added to the flask. The mixture was stirred at 35 °C overnight. After the elimination of DMF under reduced pressure, 15 mL of toluene was added to the flask, and the insoluble salt (NaBr) was removed by centrifugation (5 000 rpm for 15 min). The copolymer was recovered by the evaporation of solvent under reduced pressure. No obvious ^{1}H NMR chemical shift difference was observed between **SBC-γN_3** and **SBC-γBr**. FT-IR confirmed the presence of a peak at 2 096 cm^{-1} related to the azide stretch; (KBr) 1/λ [cm^{-1}]: 2 919 (s), 2 859 (s), 2 096 (s, azide band), 1 725 (s), 1 668 (s), 1 445 (s), 958 (m), 863 (s), 735 (s), 657 (m).

4.2.6. Synthetic Modification of α-N_3-Three Arm SBC to α-Cholesteryl-Three Arm SBC: Star-Poly(ε-CL-co-α-cholesteryl 5-hexynoate-ε-CL-co-DL-LA), (SBC-αCLC) *via* Azide-Alkyne Huisgen Cyclo-Addition Reaction (Click Reaction)

In a round bottom flask 1 equivalent of **SBC-αN_3** (1.5 g, 33.0 mmol) was dissolved in freshly distilled THF, then 1.2 equivalent of cholesteryl 5-hexynoate **1** (1.94 g, 4.03 mmol), 0.1 molar equivalent of copper iodide (0.06 g, 0.33 mmol), and 0.1 molar equivalent of triethylamine (0.03 g, 0.33 mmol) were added. The mixture stirred overnight at 35 °C under nitrogen. Then, the solvent was evaporated under reduced pressure. The residual mixture was dissolved in dichloromethane and was centrifuged to remove unreacted materials and side products. The final purified product was characterized using ^{1}H NMR and FT-IR. ^{1}H NMR ($CDCl_3$, 400 MHz) δ[ppm]: 7.54 (s, C*H*═C-triazole), 5.43–5.34 (m, C═C*H* cholesterol), 5.10–5.06 (m, COC*H*CH_3), 4.68–4.55 (m, O−C*H* cholesterol), 4.24–4.19 (m, CH_2O), 4.18–4.13 (t, $J = 5.0$ Hz, CH_2O), 4.11–4.05 (t, $J = 4.4$ Hz, CH_2O), 2.47–2.41 (t, $J = 4.9$ Hz, COCH_2), 2.31–2.25 (m, COCH_2), 2.07–1.02 (m, CH_2, CH_3), 1.05–1.03 (s, CH_2, CH_3),

0.96–0.92 (d, $J = 3.3$ Hz, CH_2, CH_3), 0.91–0.87 (dd, $J = 1.9$, $J = 1.8$, CH_3), 0.71–0.68 (s, CH_3). ^{13}C NMR ($CDCl_3$, 100 MHz): δ 172.53, 139.64, 122.68, 74.01, 69.05, 56.69, 56.12, 50.01, 42.31, 39.73, 38.13, 36.98, 36.60, 36.18, 35.80, 33.32, 31.91, 28.24, 27.80, 24.29, 23.83, 22.84, 22.57, 19.33, 18.72,17.87, 16.78, 11.86. FT-IR (KBr) 1/λ [cm^{-1}]: 3 260 (s), 2 920 (s), 1 710(s), 1 460 (s), 1 370 (s), 1 240(m), 1 190(s), 733(s), and 668(s). Glass transition temperature (T_g) was found at –21.60 °C, and decomposition temperature at 245.8 °C.

4.2.7. Synthetic Modification of γ-N_3-Three Arm SBC to γ-Cholesteryl-Three Arm SBC: Poly(ε-CL-co-γ-Cholesteryl 5-Hexynoate-ε-CL-co-DL-LA), (SBC-γCLC) by Click Reaction

In a round-bottom flask **SBC-γN_3** (1.5 g, 0.70 mmol) was dissolved in 15 mL dry DMF. Then, cholesteryl 5-hexynoate **1** (0.4 g, 0.832 mmol, 1.2 equiv.), CuI (0.0132 g, 0.069 mmol, 0.1 equiv.), and triethylamine (0.07 g/9.68 μL, 0.069 mmol, 0.1 equiv.) were added to the flask. The solution was stirred overnight at 35 °C. The reaction progress was monitored by FT-IR spectroscopy after 24 h. The disappearance of the azide band at 2 096 cm^{-1} indicated that the reaction was complete. The click reaction product was precipitated in cold methanol, filtered, and dried under reduced pressure. ^{1}H NMR ($CDCl_3$, 400 MHz): δ[ppm]: 7.33 (broad s, C*H*=C-triazole), 5.39 (m, C=C*H* cholesterol), 5.16 (m, COC*H*CH_3), 4.62 (m, O—C*H* cholesterol), 4.20–4.11 (m, CH_2O), 4.16 (t, $J = 4.6$ Hz, CH_2O), 4.07 (t, $J = 4.5$ Hz, CH_2O), 2.44 (t, $J = 4.8$ Hz, COCH_2), 2.42–2.24 (m, COCH_2), 2.08–1.06 (m, CH_2, CH_3), 1.03 (s, CH_3), 0.93 (d, $J = 3.2$ Hz, C*H*), 0.90–0.86 (dd, $J = 1.8$, $J = 1.7$ CH_3), 0.69 (s, CH_3). IR (KBr) 1/λ [cm^{-1}]: 3 020 (s), 2 920 (s), 1 720 (s), 1 460 (s), 1 370 (s), 1 210 (s), 1 090 (m), 746 (s), 667 (s). Glass transition temperature (T_g): −37.10°C, TGA decomposition temperature: 235.05 °C.

4.2.8. Synthesis of α-Position LC Elastomer: Star-Poly-(ε-CL-co-α-Cholesteryl 5-Hexynoate-ε-CL-co-DL-LA), (LCEα)

Amsden's chemical cross-linking procedure to obtaine elastomers using bis-caprolactone (BCP) as cross-linker was followed.[17] To prepare the elastomer, a 3:1 mass ratio of **SBC-αCLC** to BCP and also a molar ratio of 2.3:1 for ε-CL to BCP were used (ε-CL as solvent). In a dry silanized ampoule, BCP (1.0 g) and of ε-CL (1.0 g) were mixed and heated in a sand bath to 140 °C until the BCP was dissolved. Then, **SBC-αCLC** (3.0 g) was added to the ampoule and the contents were mixed using a vortex mixer. Once the mixture was homogenous, tin(II) 2-ethylhexanoate catalyst (90 μL) was added. All contents of the ampoule were mixed using vortex and then the ampoule was flame-sealed. The closed ampoule was placed in a sand bath at 140 °C for approximately 18 h. The resulting elastomer was removed from the ampoule and washed with 70% ethanol solution to remove unreacted products and prepare for biocompability tests. The resulting elastomer was dried under vacuum before characterization using FT-IR, DSC, and TGA. FT-IR (KBr) 1/λ [cm^{-1}]: 2 950–2 870 (broad, s), 1 710 (s), 1 540 (m), 1 320–1 040 (broad, s), 958 (s), and 733 (m). Glass transition temperature (T_g): −37.20 °C, TGA decomposition temperature: 260.2 °C.

4.2.9. Synthesis of γ-Position LC Elastomer: Star-Poly(ε-CL-co-γ-Cholesteryl 5-Hexynoate-ε-CL-co-DL-LA), (LCEγ)

BCP (0.166 g) and ε-CL (0.162 g) were added to a silanized ampoule. The ampoule was purged with nitrogen and after mixing its contents with a vortex mixer it was placed in an oven at 140 °C for 10 min to allow BCP to dissolve. Then, **SBC-γCLC** (1.0 g) was transferred into the ampoule. Using a vortex mixer the ampoule contents were mixed and after adding tin(II) 2-ethylhexanoate catalyst (45 μL) the ampoule was sealed under vacuum. The sealed ampoule was heated at 140 °C in a sand bath for 48 h. The resulting elastomer was then removed, washed with 70% ethanol solution to remove unreacted products and prepare for biocompability tests. Elastomer was dried under vacuum before characterization using FT-IR, DSC, and TGA. FT-IR (KBr) 1/λ [cm^{-1}]: 2 950–2 853 (broad, s), 1 695 (s), 1 539 (m), 1 338–1 082 (broad, s), 960 (s), 735 (m). Glass transition temperature (T_g): −22.09 °C, TGA decomposition temperature: 252.3 °C.

4.3. Characterization

4.3.1. ^{1}H NMR, ^{13}C, and FT-IR

The proton and carbon NMRs spectra of all starting co-polymers were recorded in $CDCl_3$ at room temperature on a Bruker DMX 400 MHz machine and referenced internally to residual peaks at 7.26 (^{1}H). Due to insolubility of obtained elastomers, NMR was not recorded. FT-IR samples were prepared as thin film between KBr plates and spectra recorded using a Magna Nicolet-500 series FT-IR spectrometer.

4.3.2. Gel Permeation Chromatography

Molecular weight distributions of the SBCs were determined by polystyrene standards as reference material using an Agilent 1200 series liquid chromatography system equipped with refractive index and variable wavelength detector and two American Polymer Standards (Mentor, OH) linear bed GPC columns. THF was used as eluent with a flow rate of 1 ml · min^{-1}.

4.3.3. Optical Microscopy

Polarized optical microscopy (POM) observations were performed using an Olympus BX53 polarizing microscope (20×) equipped with a Linkam LTS420 heating/cooling stage, Linkam TST350 tensile testing heating/cooling stage or a Linkam CSS450 optical rheology heating/cooling stage. All samples were initially heated to isotropic phase and then cooled to observe the temperature range at a rate of 0.1 °C.

4.3.4. Florescence Confocal Microscopy

Florescence confocal microscopy was performed using an Olympus fv1000 equipped with three laser lines and cells were stained with ToPro® (nuclear, white), and DIOC6 (membrane, green) dye.

4.3.5. Small-Angle X-ray Diffraction (SAXD)

The samples were sandwiched between Kapton windows and mounted on Linkam LTS420 heating/cooling stage. SAXD data were collected using a Rigaku 3-pinhole camera (S-MAX3000) equipped with a Rigaku MicroMax + 002 microfocus sealed tube (Cu Kα radiation at $\lambda = 1.54$ Å) and Confocal Max-Flux (CMF) optics

operating at 40 W. The system is equipped with a 3-m, fully evacuated camera length. The system is also equipped with 200 mm multiwire 2D detector for data collection. We collected SAXD data $0.0044 \leq q \geq 4.76$ Å^{-1} with 300 s of exposure. The data reduction was done using Rigaku's SAXSGUI data processing software. The *d*-spacing values were calculated using Bragg's diffraction law.

4.3.6. Differential Scanning Calorimetry (DSC)

Thermal phase transitions were carried out with Thermal Perkin Elmer Pyris1 analyzer with a scanning rate of 10 °C · min^{-1} from −70 to 250 °C under nitrogen atmosphere.

4.3.7. Thermo Gravimetric Analysis (TGA)

Thermal degradation studies were carried out with Hi-Res TGA-2950 thermal analyzer (TA instruments) under nitrogen atmosphere with ramp of 10 °C per minute.

4.3.8. Scanning Electron Microscopy (SEM)

Elastomer samples were gold coated (700 Å) using a sputter coater (Hummer VI-A, Anatech Ltd, VA) at 10 mA DC for 3 min and images were acquired using a Hitachi S-2600N SEM.

4.3.9. Cell Cultures

The human neuroblastoma cell line (SH-Sy5Y) was cultured in Dulbecco's Modified Eagle Medium/F-12, (1:1, Hyclone) and C2C12 myoblasts were cultured in DMEM with 4.5 g · L^{-1} glucose and 1X Glutamax (Life Technologies). Both culture systems were supplemented with 1% penicillin/streptomycin, and 10% FBS (Hyclone) at 37 °C in 5% CO_2 in humidified air. Cells were maintained in logarithmic growth phase and sub cultivated appropriately with Trypsin-EDTA.

4.3.10. Contact Angle Measurements

Contact angle measurements of sample the surfaces were characterized by the sessile drop method using a contact angle goniometer (Rame-Hart-290, Rame-Hart, Inc., USA). An automated dispensing system was used to dispense a 2 μl droplet of deionized water on the surfaces. The water contact angle was measured 15 s after placing the droplet to allow time for equilibration.

4.3.11. Cell Seeding

Prior to seeding, elastomers were sliced using a Leica cm1950 microtome at −20 °C into 60, 100, and 200 μ to obtain discs or prepared as films. After that, elastomers (disk/films) were soaked in 70% ethanol for 20 min and then washed with PBS. In some cases, a coating of collagen or D-lysine was applied and elastomers were then exposed to UV light. Cells were collected by trypsinization and centrifugation (1 500 rpm, 5 min) and re-suspended in warm media. Then, cell suspension (about 0.5 mL) was pipetted carefully only on top of sterilized elastomer. The seeded elastomers were left for 4 h inside an incubator (at 37 °C, 5% CO_2), after that time media was added to fully submerged the seeded elastomer in media.

Acknowledgements: The authors would like to thank Dr. K. McEleney (Department of Chemistry, University of Manitoba) for his help with the SAXD measurements supported by the Canada Foundation for Innovation (CFI). We also thank the following dedicated undergraduate students for their help with the materials synthesis: Joseph Charnas, Fernando C. Barbosa, and Rory Emery. The authors would like to thank the National Science Foundation for funding the NSF-REU Program (CHE-1263087) and Kent State University for financial support of a collaborative research grant and the Regenerative Medicine Initiative at Kent State (ReMedIKS). In addition, TH gratefully acknowledges financial support from the Government of Ohio's Third Frontier Program for Ohio Research Scholars. The name of author B.-W. Park was amended on February 11, 2015.

Received: July 10, 2014; Revised: September 2, 2014; Published online: October 10, 2014; DOI: 10.1002/mabi.201400325

Keywords: liquid crystal elastomers cell scaffolds

[1] a) E. Khor, L. Y. Lim, *Biomaterials* **2003**, *24*, 2339; b) H. J. Chung, T. G. Park, *Adv. Drug Deliv. Rev.* **2007**, *59*, 249; c) D. F. Williams, *Biomaterials* **2008**, *29*, 2941.
[2] M. Marcacci, E. Kon, V. Moukhachev, A. Lavroukov, S. Kutepov, R. Quarto, M. Mastrogiacomo, R. Cancedda, *Tissue Eng.* **2007**, *13*, 947.
[3] X. H. Liu, X. B. Jin, P. X. Ma, *Nat. Mater.* **2011**, *10*, 398.
[4] S. M. Willerth, S. E. Sakiyama-Elbert, StemBook, ed. The Stem Cell Research Community, StemBook, doi/10. 3824 /stembook. 1.1.1, http://www.stembook.org.
[5] For a recent review, see E.-V. Fleischmann, R. Zentel, *Angew. Chem. Int. Ed.* **2013**, *52*, 8810.
[6] a) See for example H. R. Brand, H. Finkelmann, Physical Properties of Liquid Crystalline Elastomers. In: "*Handbook of Liquid Crystals,*", 1st edition, J. W. Goodby, D. Demus, G. Gray, H-. W. Spiess, V. Vill, Eds., Vol. *3*: High Molecular Weight Liquid Crystals Wiley-VCH, Weinheim **1998**, p. 277; b) P.-G. De Gennes, M. Hébert, R. Kant, *Macromol. Symp.* **1997**, *113*, 39; c) M.-H. Li, P. Keller, *Phil. Trans. R. Soc. A* **2006**, *364*, 1847; d) S. J. Woltman, G. D. Jay, G. P. Crawford, *Nat. Mater.* **2007**, *6*, 929.
[7] a) See for example N. Herzer, H. Guneysu, D. J. D. Davies, D. Yildirim, A. R. Vaccaro, D. J. Broer, C. W. M. Bastiaansen, A. P. H. J. Schenning, *J. Am. Chem. Soc.* **2012**, *134*, 7608; b) C. Ohm, M. Brehmer, R. Zentel, *Adv. Mater.* **2010**, *22*, 3366.
[8] a) See for example C. Artal, M. B. Ros, J. L. Serrano, N. Pereda, J. Etxebarría, C. L. Folcia, J. Ortega, *Macromolecules* **2001**, *34*, 4244; b) J. Naciri, A. Srinivasan, H. Jeon, N. Nikolov, P. Keller, B. R. Ratna, *Macromolecules* **2003**, *36*, 8499; c) M. Camacho-Lopez, H. Finkelmann, P. Palffy-Muhoray, M. Shelley, *Nat. Mater.* **2004**, *3*, 307; d) E.-K. Fleischmann, H.-L. Liang, N. Kapernaum, F. Giesselmann, J. Lagerwall, R. Zentel, *Nat. Commun.* **2012**, *3*, 1178.
[9] H. Finkelmann, S. T. Kim, A. Muñoz, P. Palffy-Muhoray, B. Taheri, *Adv. Mater.* **2001**, *13*, 1069.
[10] M. Yamada, M. Kondo, J. Mamiya, Y. Yu, M. Kinoshita, C. J. Barrett, T. Ikeda, *Angew. Chem. Int. Ed.* **2008**, *47*, 4986.
[11] Y. Martin, P. Vermette, *Biomaterials* **2005**, *26*, 7481.
[12] B. Amsden, *Soft Matter* **2007**, *3*, 1335.
[13] C. Sinturel, M. Vayer, M. Morris, M. A. Hillmyer, *Macromolecules* **2013**, *46*, 5399.
[14] Y. K. Han, P. Edelman, S. Huang, *J. Macromol. Sci., Pure Appl. Chem.* **1988**, *A25*, 847.

[15] H. El-Laboudy, M. A. Shaker, H. M. Younes, *Soft Mater.* **2011**, *9*, 409.
[16] a) M. P. Hiljanen-Vainio, P. A. Orava, J. V. Seppala, *J. Biomed. Mater. Res.* **1997**, *34*, 39; b) A. J. Nijenhuis, D. W. Grijpma, A. J. Pennings, *Polymer* **1996**, *37*, 2783.
[17] H. M. Younes, E. Bravo-Grimaldo, B. G. Amsden, *Biomaterials* **2004**, *25*, 5261.
[18] R. F. Storey, S. C. Warren, C. J. Allison, A. D. Puckett, *Polymer* **1997**, *38*, 6295.
[19] M. Lang, R. P. Wong, C. C. Chu, *J. Polym. Sci. Part A: Polym. Chem.* **2002**, *40*, 1127.
[20] B. Nottelet, C. Di Tommaso, K. Mondon, R. Gurny, M. Möller, *J. Polym. Sci. Part A: Polym. Chem.* **2010**, *48*, 3244.
[21] J. Seppälä, *Stud. Mechnobiol. Tissue Eng. Biomater.* **2011**, *8*, 409.
[22] L. Jia, A. Cao, D. Levy, B. Xu, P. Albouy, X. Xing, M. J. Bowick, M. Li, *Soft Matter* **2009**, *5*, 3446.
[23] L. Jia, M. Liu, A. Di Cicco, P. Albouy, B. Brissault, J. Penelle, S. Boileau, V. Barbier, M. Li, *Langmuir* **2012**, *28*, 11215.
[24] R. Pinol, L. Jia, F. Gubellini, D. Levy, P. Albouy, P. Keller, A. Cao, M. Li, *Macromolecules* **2007**, *40*, 5625.
[25] S. Ahn, M. Gopinadhan, P. Deshmukh, R. K. Lakhman, C. O. Osuji, R. M. Kasi, *Soft Matter* **2012**, *8*, 3185.
[26] P. Deshmukh, S. Ahn, D. M. Geelhand, R. M. Kasi, *Macromolecules* **2013**, *46*, 8245.
[27] D. L. Thomson, III, P. Keller, J. Naciri, R. Pink, H. Jeon, D. Shenoy, B. R. Ratna, *Macromolecules*, **2001**, *34*, 5868.
[28] For a recent example, seeW. Zang, D. S. Choi, Y. H. Nguyen, J. Chang, L. Qin, *Sci. Reports* **2013**, *3*, 2332.
[29] a) S. Guruvenket, G. M. Rao, M. Komath, A. M. Raichur, *Appl. Surf. Sci.* **2004**, *236*, 278; b) P. A. Ramires, L. Mirenghi, A. R. Romano, F. Palumbo, G. Nicolardi, *J. Biomed. Res.* **2000**, *51*, 535; c) T. G. van Kooten, H. T. Spijker, H. J. Busscher, *Biomaterials* **2004**, *25*, 1735.
[30] a) N. A. Lockwood, J. C. Mohr, L. Ji, C. J. Murphy, S. R. Palecek, J. J. de Pablo, N. L. Abbott, *Adv. Funct. Mater.* **2006**, *16*, 618; b) A. M. Lowe, N. L. Abbott, *Chem. Mater.* **2012**, *24*, 746.